

INSTITUT NATIONAL DE RECHERCHE ET DE SECURITE
Centre de Recherche
Département "Environnement Physique"
Service "Thermique, Ventilation, Eclairage"
Avenue de Bourgogne
B.P. 27
54501 Vandoeuvre Cédex FRANCE

3203

Projet de Publication n° 1343

Avril 1987

**DYNAMICAL AND CONTAMINANT FLOW SIMULATION INSIDE VENTILATED INDUSTRIAL
PREMISES 2 : EXPERIMENTAL METHODS**

P. GARDIN
P. BERLANDIER
J.C. SERIEYS

"Document diffusé pour raison de service aux services publics et aux instances de la Sécurité Sociale mandatées pour la prévention des accidents du travail et des maladies professionnelles. Il peut être utilisé par eux, sans réserve, comme document de travail interne ou pour des réunions qu'ils provoqueraient. Il ne peut, en revanche, être placé en l'état dans les circuits documentaires car il fera ultérieurement l'objet d'une publication dans une revue".

• Diffusion externe :

- C.N.A.M. (2)
- C.R.A.M.(2)
- C.G.S.S.(2)
- Ministère des Affaires Sociales et de la Solidarité Nationale (DRT - DSS)
- Directions Régionales du Travail et de la Main d'Oeuvre

• Diffusion interne :

- P / DG - DER - ETA - EG - INF - DN - FOR - SM
- N / DER - DS - DN - EP - Chrono

SIMULATION DE LA DYNAMIQUE DE L'ÉCOULEMENT ET DE LA DISPERSION D'UN POLLUANT A L'INTERIEUR D'UN LOCAL INDUSTRIEL VENTILE

2 - Méthodes expérimentales

P. GARDIN, P. BERLANDIER, J.C. SERIEYS

Service Thermique, Ventilation, Eclairage, INRS, avenue de Bourgogne, B.P. 27, 54501 Vandoeuvre Cédex France

Résumé du projet de publication n° 1343

Afin de valider un code numérique destiné au calcul des vitesses et des concentrations locales à l'intérieur d'une enceinte ventilée soumise à une source polluante, une similitude hydraulique a été développée.

L'étude est séparée en deux parties :

- 1) Mise en oeuvre d'une technique de mesure de concentration par conductimétrie
- 2) Mise en oeuvre d'une technique de mesure de vitesse par anémométrie laser

La communication décrit chacun des deux bancs hydrauliques ainsi que les techniques de mesure utilisées.

Des comparaisons entre les résultats expérimentaux et les résultats numériques sont ensuite présentées :

- pour les concentrations, on superpose plusieurs profils verticaux de concentration prédits et mesurés. L'accord est de l'ordre de 10 % sauf dans la région directement en aval de la source d'émission du polluant où l'accord est de l'ordre de 30 % ;
- pour les mesures de vitesse, on détermine expérimentalement le champ de vitesse dans le plan de symétrie de la maquette par une centaine de points. Des profils spécifiques ont été choisis à des fins de comparaison avec les résultats du calcul numérique bi-dimensionnel. Les différences relatives obtenues sont de 30 % environ.

"AIR DISTRIBUTION IN VENTILATED SPACES"

International Conference

Stockholm 10-12 juin 1987

DYNAMICAL AND CONTAMINANT FLOW SIMULATION INSIDE VENTILATED INDUSTRIAL PREMISES 2 : EXPERIMENTAL METHODS

P. GARDIN, P. BERLANDIER, J.C. SERIEYS

Service Thermique, Ventilation, Eclairage, INRS, avenue de Bourgogne, BP 27, 54501 Vandoeuvre Cédex, France

A - INTRODUCTION

The purpose of this paper is to get the experimental concentration field and the experimental mean flow inside a scale model to study the general structure of contaminant flows inside ventilated industrial premises.

The two main points of the work are :

- performing reliable measurements of contaminant concentrations and mean velocities inside the experimental model of industrial room ;
- studying the validity of numerical results concerning the same problems.

For clarity, we choose to split the concentration study from the dynamical study :

Part I "Contaminant flow simulation inside industrial premises"

Part II "Mean flow simulation inside industrial premises"

Those two programmes will be performed inside two different hydraulic benches.

B - PART I "CONTAMINANT FLOW SIMULATION INSIDE INDUSTRIAL PREMISES"

Contents

- 1 - Presentation of the hydraulic testing bench - Measurement technique
 - 1.1 - Hydraulic bench
 - 1.2 - Hydraulic model
 - 1.3 - Measurement system
 - 1.4 - Conductivity probe
 - 1.5 - Acquisition apparatus
- 2 - Experimental results
 - 2.1 - Running parameters
 - 2.2 - Testing experiments and results
 - 2.3 - Experimental uncertainties
- 3 - Conclusion
- 4 - Bibliography and references
- 5 - Acknowledgements

1 - Presentation of the hydraulic testing bench - Measurement technique

1.1 - Hydraulic bench

To have reliable experimental results it is necessary to control the parameters involved in our problem : flow-rates and temperatures of incoming fluid and emitted contaminant. Therefore we can distinguish three circuits in our testing bench (Fig 1) :

- a water circuit whose parts are :
 - . a filter (porosity diameter : 30 μ m) ①
 - . a buffer tank (500 l) with an immersed resistance (2400 W) to heat water as fast as possible ②

- . an adjustment tank (500 l) with a thermostatisation system to adjust the water temperature to the required value ($20^{\circ}\text{C} \pm 0,3^{\circ}\text{C}$) ③
- . an hydraulic pump to circulate the fluid ④
- a contaminant (salt water) circuit whose parts are :
 - . a buffer tank (200 l) ⑤
 - . an adjustment tank with a thermostatisation system ($20^{\circ}\text{C} \pm 0,5^{\circ}\text{C}$) ⑥
 - . a tank with a constant level of salt water (salt water flows out by gravity) ⑦
 - . an hydraulic pump to homogenize temperature and to avoid salt stratification ⑧
 - . a cock to regulate salt water flow-rate ⑨
 - . a rotameter ⑩
- an extracted fluid circuit whose parts are :
 - . an hydraulic pump to extract fluid from the model ⑪
 - . a graduated tank to measure -with a chronometer- the flow-rate of extracted fluid ⑫

The use of salty solution -water with KCl- involves unoxydizable material supports (PVC, altuglass).

Since salt cannot be separated from the extracted fluid, there is no loop circuit and the extracted fluid goes to the sewage system ⑬ .

1.2 - Hydraulic model

The hydraulic model is immersed in water. It has been made with altuglass and has a parallelepipedic geometry.

Main parts of it are (Fig 2) :

- the inlet of water which is a rectangular slot ($5 \times 180 \text{ mm}^2$) ① ,
- the outlet of extracted fluid (rectangular slot : $1 \times 180 \text{ mm}^2$) ② ,
- the inlet of contaminant (rectangular slot : $1 \times 180 \text{ mm}^2$) ③ .

The model is built such that, in the median plane P1, boundary effects can be considered as negligible : in P1, the concentration distribution is two-dimensional. Measurements have been performed in the P1 plane.

There is a sliding channel (④) in the upper side of the model. Thus, we can measure throughout P1. A stuffing box warrants the water-tightness when the probe passes through the upperside.

1.3 - Measurement system

The conductivity of electrolyte solutions depends on both temperature and concentration. Since the temperature of the solution is constant in our case, it can be expected that the conductivity will depend only on the concentration of salt in water.

When we introduce an electrode -the conductivity probe- and a counter electrode in the model, and put them up to two different potentials, the current going from an electrode to the other can be first measured [1]. We then deduce the conductivity of the fluid between the two electrodes and, accordingly, the electrolyte concentration.

It has been shown that, by making one electrode -the probe- much smaller than the other one, the conductivity of the solution is measured only in the vicinity of the smallest electrode [2]. In this way, we have access to the local concentration measurements.

An alternating voltage is applied between the electrodes to enhance the electrochemical reaction. And we can summarize the measurement system in the following way [3] :

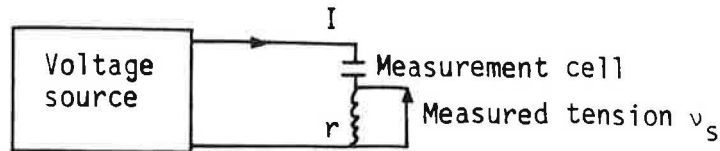


Figure 3 : Measurement system

The current I flowing through the circuit is obtained by measuring the voltage at the ends of a resistance r .

The concentration is deduced from v_s by calibration curves. These are established from reference concentration electrolytes. Below a fixed value (1 g/l in our case) the relation between concentration and tension is linear (Fig 4).

1.4 - Conductivity probe

The probe has been made in our laboratory according to designs from previous studies [3], [4].

It consists of a platinum wire -30 μm diameter- encased in a small conic tapered capillary of rigid plastic (Fig 5).

Although we tried to build the probe as small as possible, its introduction in the model will disturb the flow in an unknown way.

To avoid partially the drift problem of the probe response in time, one can platinize the probe : a small sheet of platinum is electrochemically deposited on the conductivity probe tip [3].

It is possible to put up with the drift by controlling it : from time to time, we note the tension obtained with a known concentration, calculate -by difference- the drift and add it to the mean values (with, of course, a ponderation coefficient to take into account the linear decrease of the probe response between the two checking times).

1.5 - Acquisition apparatus

The signal is sent from the conductivity probe to a voltmeter (7061 solartron). Each mean value was obtained from 620 data sampled during 56 s.

The voltmeter was remotely controlled (via an IEEE interface) by a Hewlett-Packard 85 micro-computer.

2 - Experimental results

2.1 - Running parameters

Experimental characteristics of the flow were :

- temperature of water : 20°C
- temperature of salt water : 20°C
- flow-rate of extracted fluide : 7,5 l/mn
- flow-rate of salt water : 0,45 l/mn
- concentration of salt water at the emission line : \approx 2,5 g/l
- Reynold number : 19440

(the characteristic length is the height of the model and the characteristic velocity is the incoming water velocity).

Concentrations were normalized by the exhaust concentration. We have 113 measurements points localized in the measurement plane P1 (Fig 6). These points are close to each other where concentration gradients are supposed to be high and near the exhaust.

2.2 - Testing experiments and results

Tests were carried out to check the validity of the two basic assumptions : two-dimensional flow and passive contaminant.

In a first time, we showed that no change was observed in the concentration field for measurements performed in plane close and parallel to P1 (cf Fig 2). Thus, we have a two-dimensional concentration field in the measurement sheet.

Then, by increasing progressively the contaminant flow-rate, we realized that the nondimensional concentration field displayed no significant change until the contaminant flow-rate was about 0,8 l/mn. Accordingly, the contaminant can be considered as passive in our experiment.

In figures 7 to 12, we have drawn together experimental vertical concentration profiles and predictions obtained in the same configuration with a numerical model [5].

As can be seen from these figures, for most points the agreement is better than 20 %.

2.3 - Experimental uncertainties

Two types of uncertainty are involved here :

- an uncertainty due to the fact that the mean value is not obtained within an infinite time ; thus, the time average doesn't converge exactly to the actual mean value ; the lack of accuracy depends on the location of the measurement point.
- an uncertainty as a result that the running parameters -flow-rates of water and salt water, exact location of measurement points- cannot be precisely controlled from an experiment to an other ; small bubbles can also appear on the walls of the model and disturb the fluid flow, mainly if the bubbles are located just downstream the contaminant emission line.

Respective uncertainties are estimated by :

- repeating continuously in time the mean value measurement (keeping constant the running parameters) at some characteristic points (table 1) ;
- repeating each day the mean value measurement (trying to keep constant the running parameters from one day to the other) at some characteristic points (table 2).

The addition of the two types of uncertainty gives an estimation of the total uncertainty.

Different relative uncertainty regions can be roughly defined (Fig 13).

Comparison between numerical and experimental results, taking into account those uncertainties can be carried out for profiles located, for instance, upstream and downstream the emission line (Fig 7 and 10).

3 - Conclusion

Our results display a good quantitative agreement between experiment and prediction.

From a ventilation point of view, it can be emphasized that all parts of the model are contaminated, except in the inlet region. Upstream the emission line and in the central region, the concentration is almost uniform and equal to the outlet concentration. The highest concentrations are located downstream, up to the outlet.

The measurement method gives reliable results, and we can expect that it will be an efficient support for further developpements in ventilation.

4 - Bibliography and references

- [1] C.H. GIBSON and W.H. SCHWARZ "Detection of conductivity fluctuations in a turbulent flow field", J. Fluid Mechanics 16, p 357 (1963)
- [2] J. NEWMAN "Resistance for flow of current to a disk" J. of the Electrochem soc. 113, p 501 (1966)
- [3] J.F. BRODBERGER "Étude expérimentale des phénomènes de mélange en phase liquide : cas du mélangeage turbulent de fluides non réactifs", Ph.D. thesis, INPL-NANCY (1981)
- [4] R.S. TORREST and W.E. RANZ "Concentration fluctuations and chemical conversion associated with mixing in same turbulent flow", A.I.Che. J. 16 p 930 (1970)
- [5] J.R. FONTAINE and F. DELLAGI "Dynamical and contaminant flow circulation inside ventilated industrial premises 1 : numerical methods". Submitted to this conference.

5 - Acknowledgements

We are grateful to Professor G. COGNET for mentioning to us the conductivity method as a reliable scheme in contaminant flow simulation problem.

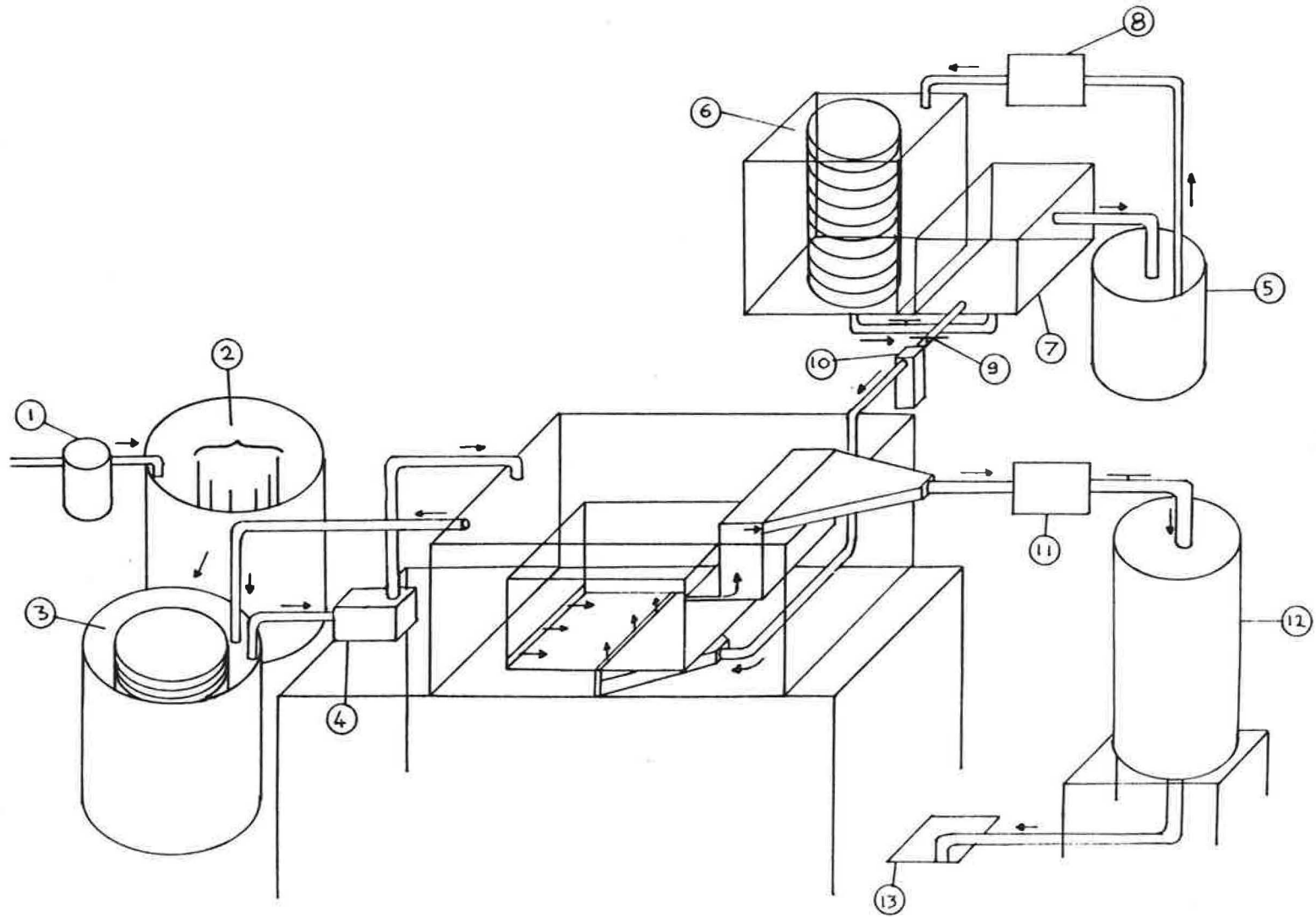


Fig 1 : Hydraulic bench

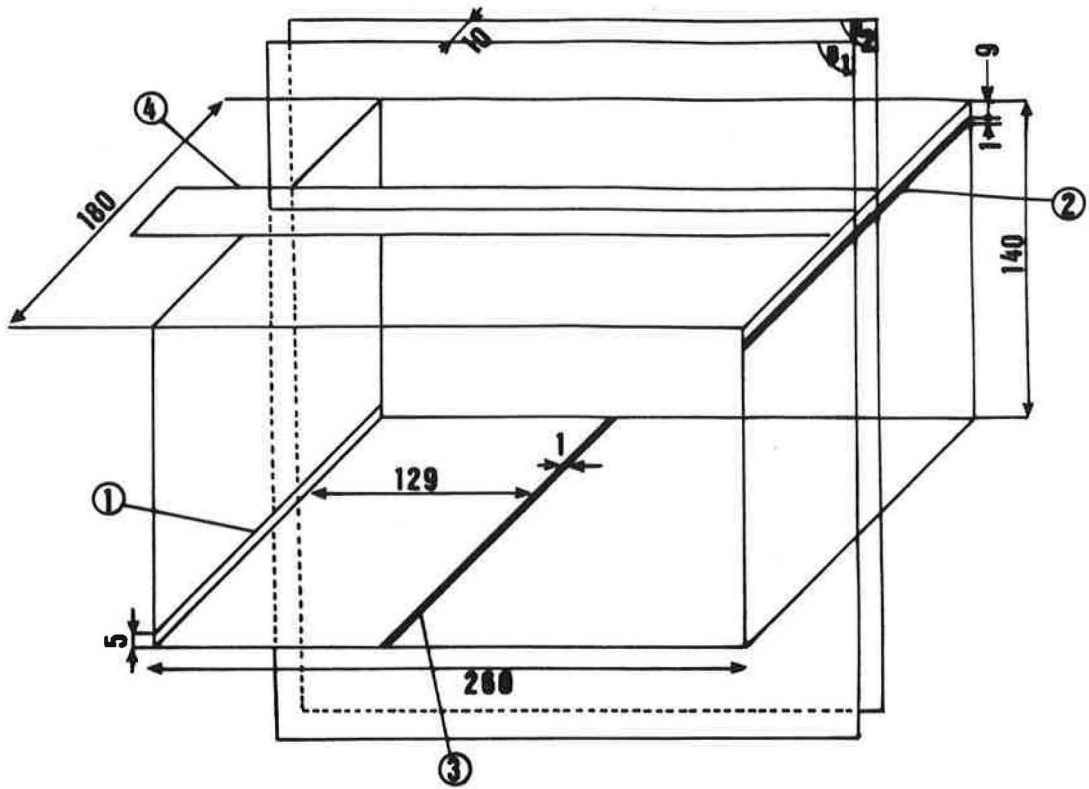


Fig 2 : Hydraulic model

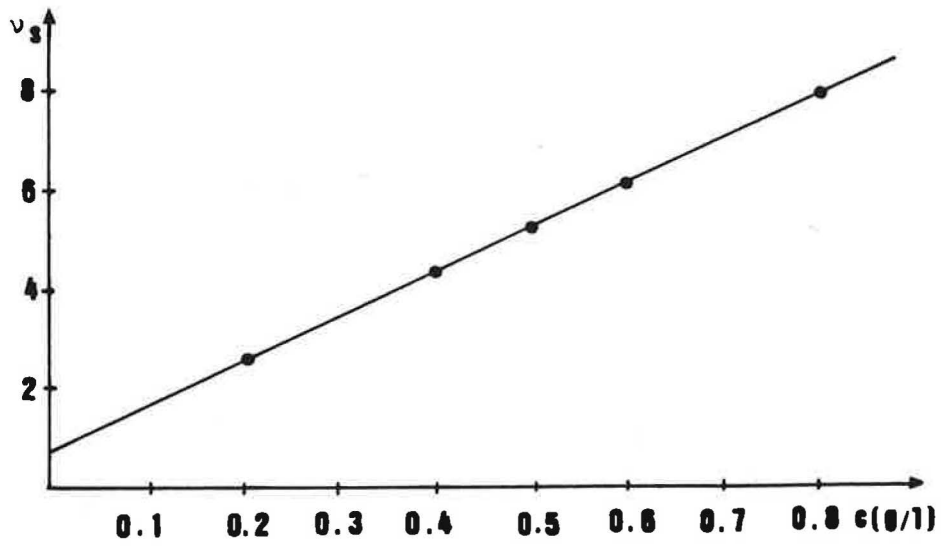


Fig 4 : Calibration curve

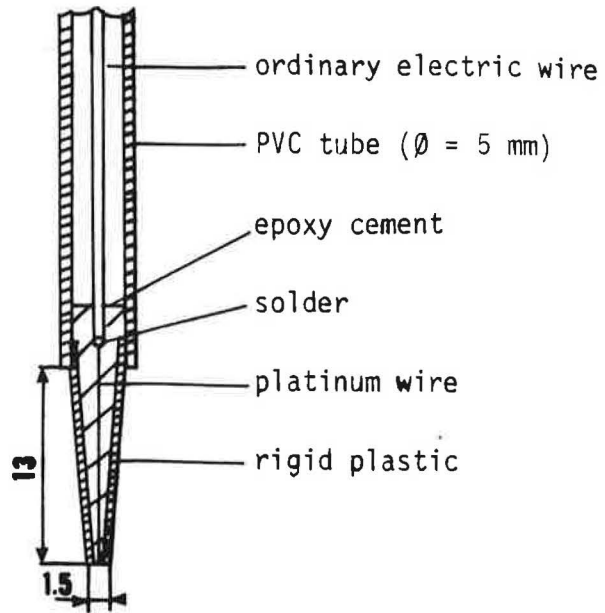


Fig 5 : The conductivity probe

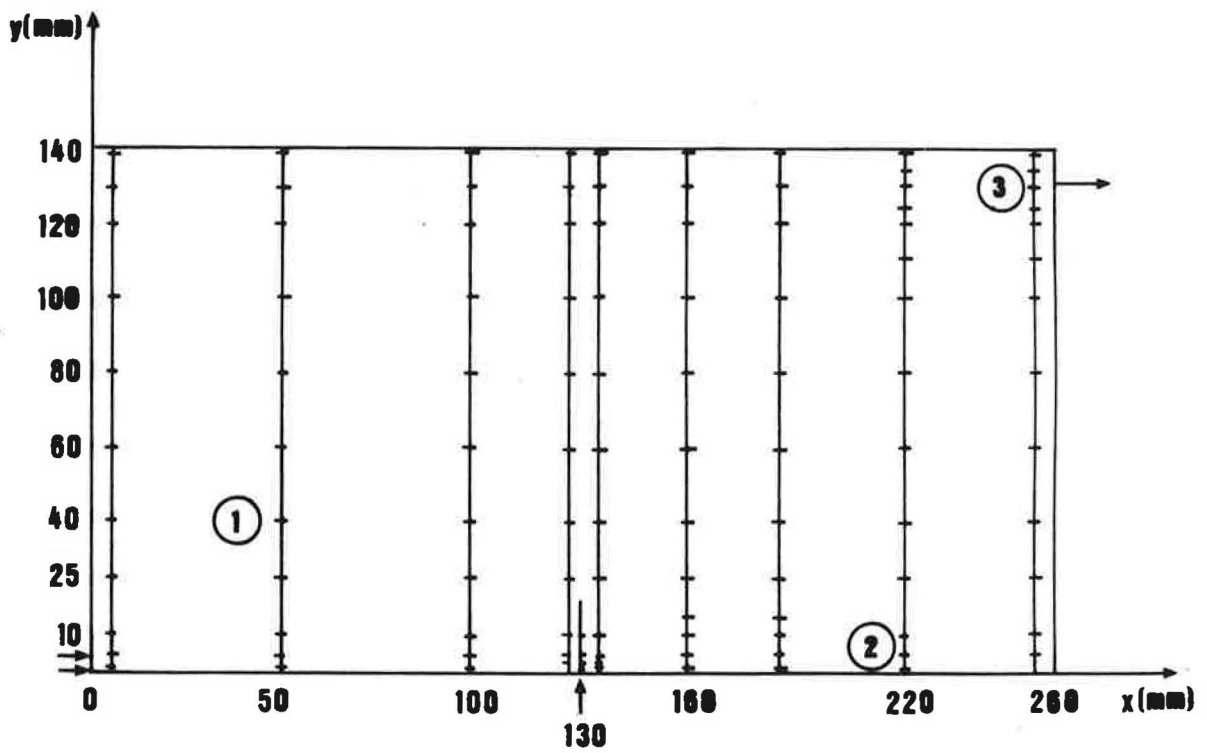


Fig 6 : Measurement points (in P1 plane)

Vertical concentration profiles

Concentrations \tilde{C} are normalized by the exhaust concentration.
Lengths (\tilde{X}, \tilde{Y}) are normalized by the height of the cavity.

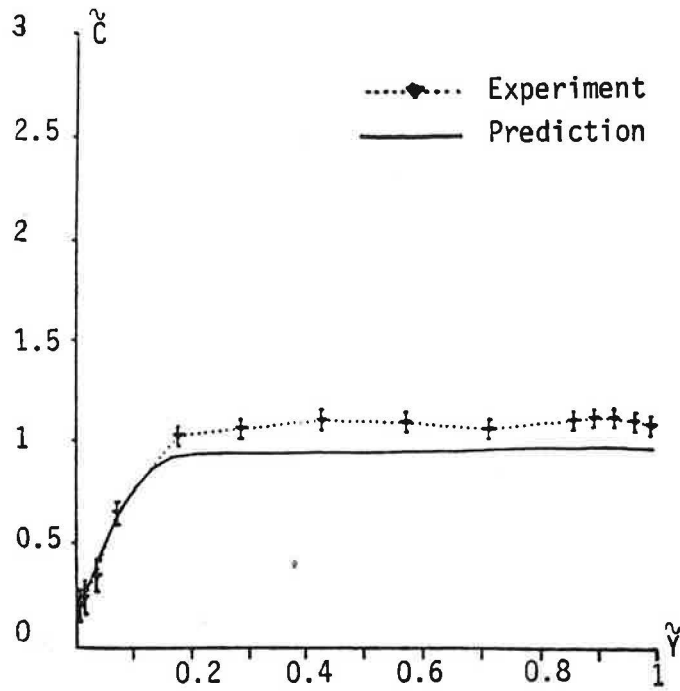


Fig 7 : $\tilde{X} = .36$

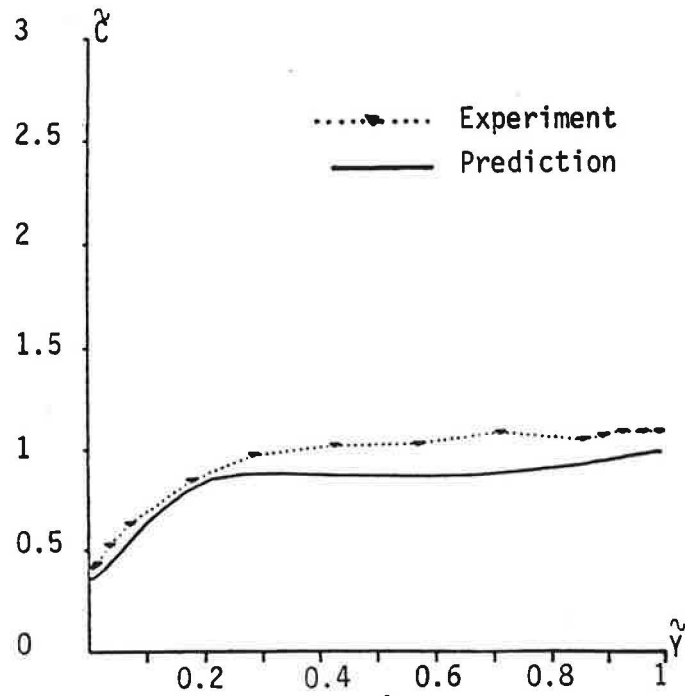


Fig 8 : $\tilde{X} = .91$

Vertical concentration profiles

Concentrations \tilde{C} are normalized by the exhaust concentration.
Lengths (\tilde{X}, \tilde{Y}) are normalized by the height of the cavity.

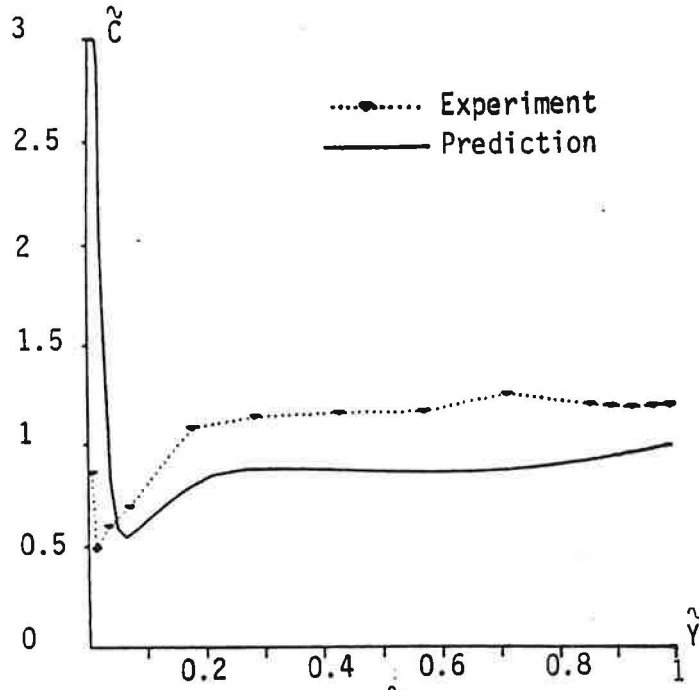


Fig 9 : $\tilde{X} = .97$

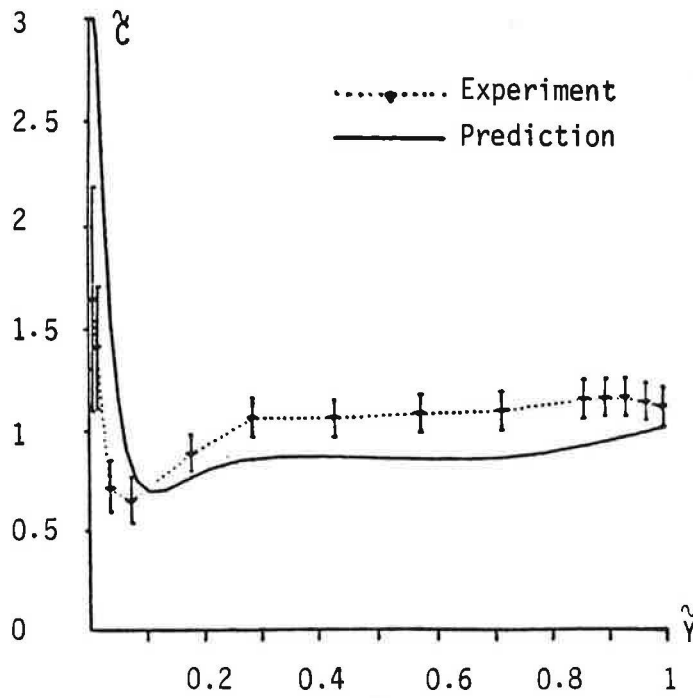


Fig 10 : $\tilde{X} = 1.14$

Vertical concentration profiles

Concentrations \tilde{C} are normalized by the exhaust concentration.
Lengths (\tilde{X}, \tilde{Y}) are normalized by the height of the cavity.

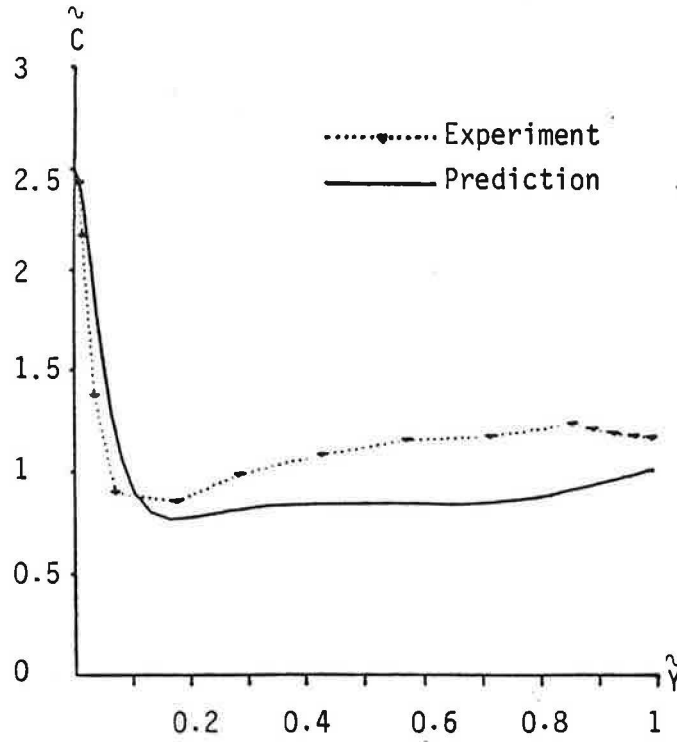


Fig 11 : $\tilde{X} = 1.32$

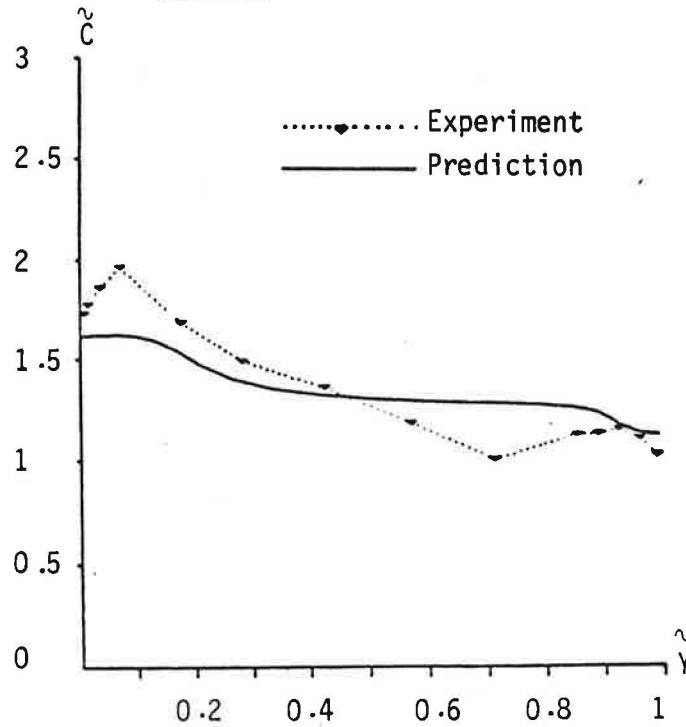
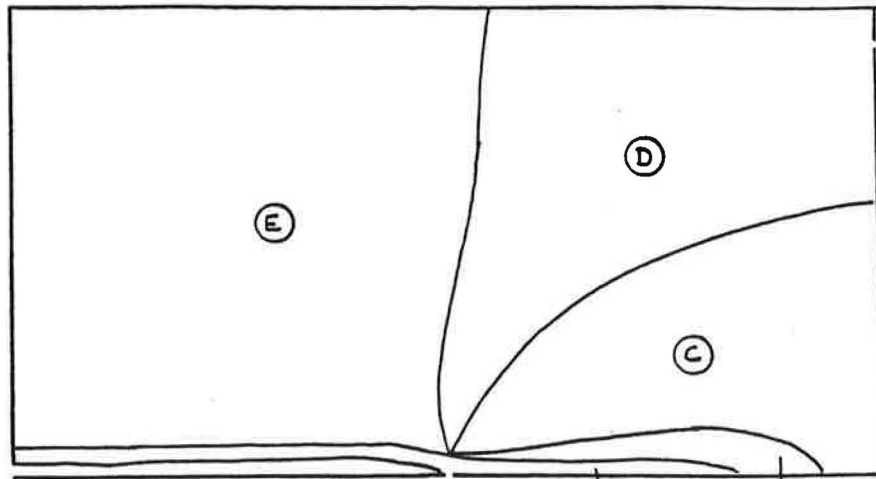


Fig 12 : $\tilde{X} = 1.33$



- A : relative uncertainty = 35 %
- B : relative uncertainty = 25 %
- C : relative uncertainty = 15 %
- D : relative uncertainty = 10 %
- E : relative uncertainty = 5 %

Fig 13 : Uncertainty regions

Table 1

Point number : 1 (for the location of the points, see Fig 6)

Experiment	1	2	3	4	5	6	7	8	9	10	\bar{c}	$\frac{\sigma_{\bar{c}}}{\bar{c}}$
Mean value	1.09	1.07	1.08	1.08	1.08	1.07	1.08	1.10	1.08	1.07	1.08	1 %

where \bar{c} = the average over the 10 values

$\sigma_{\bar{c}}^2$ = the variance over the 10 values

Point number : 2

Experiment	1	2	3	4	5	6	7	8	9	10	\bar{c}	$\frac{\sigma_{\bar{c}}}{\bar{c}}$
Mean value	2.07	2.04	2.07	2.06	2.04	1.98	1.93	1.74	1.92	1.93	1.98	5 %

Point number : 3

Experiment	1	2	3	4	5	6	7	8	9	10	\bar{c}	$\frac{\sigma_{\bar{c}}}{\bar{c}}$
Mean value	1.04	1.06	1.09	1.08	1.15	1.08	1.13	1.12	1.10	1.08	1.09	3 %

Table 2

X = 50 mm

date	Y (mm)	1	5	10	25	40	60	80	100	120	130	139
06.01.87		0.20	0.34	0.65	1.02	1.06	1.10	1.09	1.07	1.11	1.13	1.09
15.01.87		0.05	0.33	0.51	1.00	1.03	1.05	1.07	1.07	1.07	1.07	1.04

X = 160 mm

date	Y (mm)	1	5	10	15	25	40	60	80	100	120	130	139
26.12.86		1.64	0.71	0.65	0.74	0.88	1.06	1.04	1.08	1.09	1.15	1.16	1.12
12.01.87		1.18	0.60	0.64	0.70	0.89	1.06	1.02	1.06	1.06	1.08	1.10	1.08
13.01.87		1.45	0.68	0.67	0.71	0.87	1.08	1.11	1.13	1.13	1.15	1.15	1.16

Point number : 1

Date	06.01.87	12.01.87	13.01.87
Mean value	1.06	1.08	1.06

Point number : 2

Date	06.01.87	10.01.87	12.01.87	13.01.87
Mean value	2.04	1.98	1.79	1.70

Point number : 3

Date	06.01.87	12.01.87	13.01.87
Mean value	1.14	1.09	1.09

C - PART II "MEAN FLOW SIMULATION INSIDE INDUSTRIAL PREMISES"

Contents

- 1 - The hydraulic bench
 - 1.1 - Description of the bench
 - 1.2 - The scale model of the factory room
- 2 - The laser doppler anemometer system (LDA)
 - 2.1 - The doppler frequencies measuring system
 - 2.2 - The 3-D displacement system
 - 2.3 - The computing system
- 3 - Running the experiment
 - 3.1 - Use of the LDA velocimeter
 - 3.2 - Measuring the two components of the mean flow
 - 3.3 - Data acquisitions
 - 3.4 - Getting rid of the "false frequencies"
 - 3.5 - Computing the results
- 4 - A first simulation
 - 4.1 - Definition of the flow
 - 4.2 - Measurement settings
- 5 - Main results
 - 5.1 - General view of the mean flow
 - 5.2 - Accuracy of the two-dimensional mean flow hypothesis
 - 5.3 - Turbulence in the jet flow
 - 5.4 - Study of the distribution of the flow along a vertical line in the model
- 6 - Conclusion
- 7 - References

1 - The hydraulic bench

1.1 - Description of the bench

The simulation of the actual air flow into the factory room uses another hydraulic water bench, which main parts are (Fig 1) :

A plexiglass scale model, which is the very actual reproduction of the factory room (1).

An experimental tank (2.250 x 1.750 x 1.00 mm³), on the bottom of which the model is fixed (2).

Five unsteady delivering pumps to create the main ventilation flow inside the room (3).

A big buffer tank to keep steady the static pressure and the flow during the experiment (4).

Joining pipes (5).

1.2 - The scale model of the factory room

The model is a plexiglass parallelepipedic box (525 x 260 x 280 mm³) fixed upon the lower side-light of the experimental tank.

The main flow is going through the model from an inlet-hole to an outlet-hole.

The inlet is a rectangular slot (30 x 260 mm²) at the bottom of the right side of the model.

The outlet is the same slot situated in the middle of the upper side of the model.

The dimensions of the experimental tank are large enough to ensure that the mean velocity far outside the factory is nearly 0.

Because of the geometrical symmetry of the model, the mean flow can be supposed to be two-dimensional in the vertical middle plane $P = OXY$ inside the model (this must be confirmed by experimental results).

The first experimental measurements of mean flow will be done in this symmetrical plane P (Fig 2).

2 - The laser doppler anemometer system

2.1 - The doppler frequencies measuring system [1], [2]

The experimental measurements of mean velocities components U_x and U_y inside the plane P use a laser Doppler One Component Anemometer System from DANTEC.

The system is divided in :

- a laser Spectra Physics 165,
- an optical beam system DANTEC 55 X,
- a frequency LDA Counter Processor DANTEC 55L90,
- a Bragg cell and an electronic frequency shifter (55N10).

2.2 - The 3 D-displacement system

In order to investigate the whole plane of measurements, we use a 3 D-displacement system. This displacement concerns the whole system (laser, optical velocimeter, front lens and of course measuring point).

The three displacement axes (X,Y,Z) of the system are the same as the three main axes of the model.

Laser beams are reaching the measuring point by going through large rectangular side-glasses on the corresponding sides of the experimental tank.

2.3 - The computing system

A SOLAR computer fully drives the experiment. The two main tasks of the computer are :

- driving the displacement of the measuring point inside the model,
- getting and storing the frequency datas from the counter processor.

3 - Running the experiment

3.1 - Use of the LDA velocimeter

The wavelength of the laser beam is $\lambda = 515 \mu\text{m}$ (green light) and the front lens focal length $f = 600 \text{ mm}$. The space between fringes in the measuring volume is $\delta = 10 \mu\text{m}$.

The water is seeded with aluminium particles (mean diameter = $5 \mu\text{m}$).

The density of the aluminium particles is such that the data rate of the Doppler Frequencies coming from the counter processor is 5 to 40 Herz.

3.2 - Measuring the two components of the mean flow [3], [4], [5]

The laser Doppler System is a directionnal velocimeter. It can get the component of the velocity which is perpendicular to the fringe axe of the measuring volume.

In order to get the two components U_x and U_y of the mean velocity, we use two different angular adjustments of the optical velocimeter.

For each angular position (for each component of the mean velocity), we use two different frequency shifts of the fringe plane of the measuring volume in order to get the algebraic sign of each velocity component.

3.3 - Data acquisitions

For one angular position of the velocimeter and one frequency shift of the fringe plane, the Doppler frequencies coming from the counter processor (each "good" particle going through the measuring volume delivers one Doppler frequency) are sent, via an IEEE-GPIB connexion, to the computer. The storage unit is a pack of 512 measurements. For each point, it is possible to choose the number of measuring packs.

3.4 - Getting rid of the "false frequencies"

The first elimination of "false" datas is a preliminary test executed by the counter.

At every time, the internal processor of the counter compares the average Doppler frequency (computed from the 5 last Doppler frequencies) with the average frequency (computed from the 8 last datas). If the difference ratio between those two mean values is more than 1,5 %, the last data is kept off.

Then the data list of frequencies is tested by the computer in two different ways :

- keeping off the "double happening over" frequencies : when finding two successive data in the listing, the test eliminates one of them ;
- keeping off the frequencies that would deviate too much from the computed average frequency : this test uses a discriminant frequency interval which bandwidth is four times the computed turbulent root mean square, and centered on the mean frequency value.

3.5 - Computing the results

For each measuring point, the computer gives :

The statistical estimation of the algebraic sign and the intensity of the two components U_x and U_y of the mean velocity, in the measuring plane P.

The turbulent root mean square intensities, computed from the two fluctuating velocities (u_x and u_y).

The distribution of the measurements, for each point, in the frequency space.

The draw of the mean flow map, putting all the results together on one picture.

4 - A first simulation

4.1 - Definition of the flow

The main ventilation steady flow, going through the model is :
 $Q = 2,23 \text{ dm}^3/\text{second}$.

The typical value of the velocity in the inlet (outlet) is :
 $U = Q/S = 22 \text{ cm/second}$. This corresponds to a Reynolds number of 100 000 (the reference length being the height of the model).

4.2 - Measurement settings

The inner sizes of the measuring plane P are $L_x = 525$ mm and $L_y = 275$ mm.

In this plane P, we will get :

A rectangular grid of one hundred measuring points inside the plane P (in order to give a general view of the flow inside the model). The horizontal space step of the points inside the grid is $\Delta X = 76$ mm and the vertical space step is $\Delta Y = 25$ mm. The statistical estimation is computed with two packs of measurements (1 024 frequencies).

A vertical measuring line in order to compare with the numerical results. This line is set at $X = 450$ mm, and the vertical step is $\Delta Y = 10$ mm (2 048 frequencies at each point).

Measuring points, with the laser beams going through the bottom side of the tank in order to test how reliable is the two-dimensional mean flow hypothesis (2 048 frequencies at each point).

5 - Main results

5.1 - General view of the mean flow

Figure 3 gives the one hundred experimental velocity vectors in the plane P.

The main results are :

The general flow looks like a large recirculating vortex, which size is about the whole model.

The biggest velocities are very near the four sides of the model, specially inside the boundary jet flowing along the lower horizontal side of the model.

The smallest velocities are in the very inner part of the model.

This experimental map has to be compared with the numerical map (fig 4). A quite fine agreement is found in the lower part of the model [6].

5.2 - Accuracy of the two-dimensional mean flow hypothesis

With another setting of the measuring apparatus, it is possible to get the component U_z which is perpendicular to the vertical plane OXY. Table 4 gives the results for the horizontal line along the bottom wall jet [$Y = 25$, $\Delta X = 76$ mm].

In the jet flow, we can say that the two-dimensional mean flow hypothesis is quite accurate (the U_z/U_x ratio is never more than 10 % in this part of the flow).

5.3 - Turbulence in the jet flow

At the point ($X = 100$ mm, $Z = 25$ mm), figure 6 gives the space distribution of the measured frequencies, for the first mean velocity component (angular position $\alpha = -45^\circ$).

The computed root mean square velocity is : $u_x = 4,157$ cm/sec.

That means : $u_x/U_x = 0,31$.

The flow is quite turbulent in the jet region.

5.4 - Study of the distribution of the flow along a vertical line in the model

Figure 7 gives the vertical distribution of the U_x mean velocity component along the vertical line ($X = 450 \text{ mm}$, $\Delta Z = 10 \text{ mm}$).

A first qualitative interpretation shows that the global flow running across this vertical line is non zero.

This result is also shown in figure 8, in which the adimensional comparison of both experimental and numerical vertical profiles (at $X = 450 \text{ mm}$) are displayed [6].

The differences between the two profiles might be explained by a non vanishing mean velocity component perpendicular to the measuring plane. This fact is under investigation.

6 - Conclusion

The predicted and measured velocity fields were in good agreement in the lower part of the cavity. Work in progress seeks to obtain better agreement specially in the upper part of the cavity. The two-dimensional character of the flow will be checked experimentally. Efforts will be devoted to get rid of the flow transverse to the measuring plane.

7 - References

- [1] "LDA Counter Processor", 55L90a, DANTEC, DISA Documentation Dept
- [2] "Modular Optics LDA", 55X, DANTEC, DISA Documentation Dept
- [3] "Anemometrie DOPPLER à LASER", Cours LDA III, 1-2 et 3 décembre 86, DANTEC Departement Recherche Scientifique
- [4] H.D. THOMPSON and W.H. STEVENSON "Laser velocimetry and particule sizing" Hemisphere Publishing Corporation
- [5] DRAIN I.E. "The laser doppler technique, wiley", Interscience publication, Chichester, New York, Brisbane, Toronto
- [6] J.R. FONTAINE and F. DELLAGI "Dynamical and contaminant flow simulation inside ventilated industrial premises 1 : numerical methods". Submitted to this conference

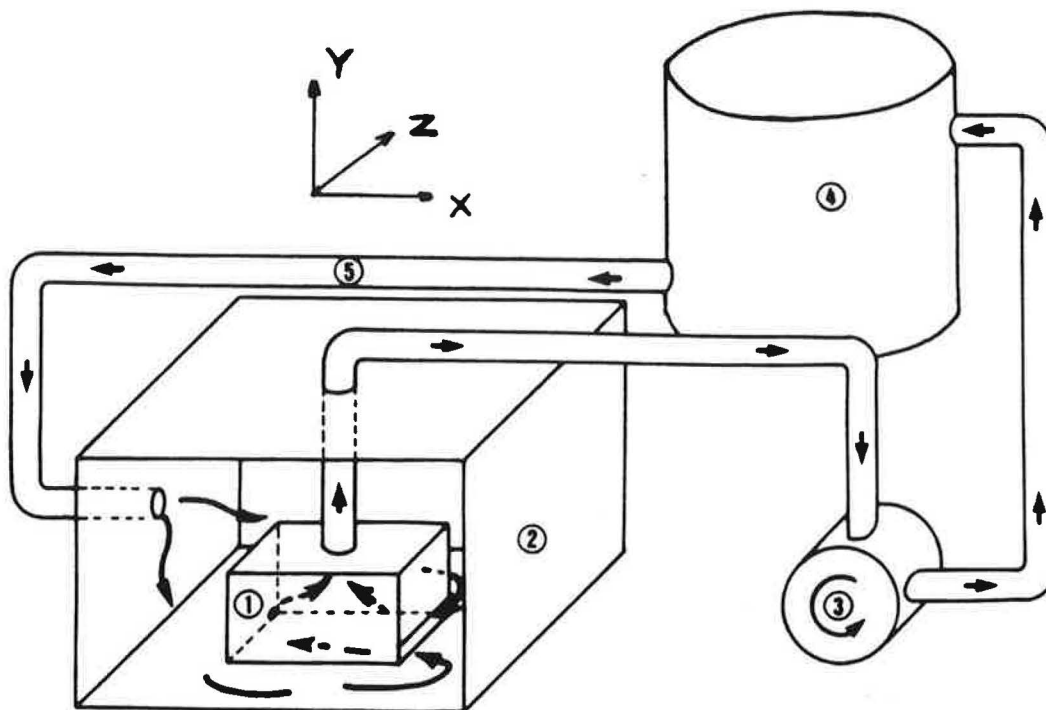


Fig 1 : Main view of the hydraulic bench

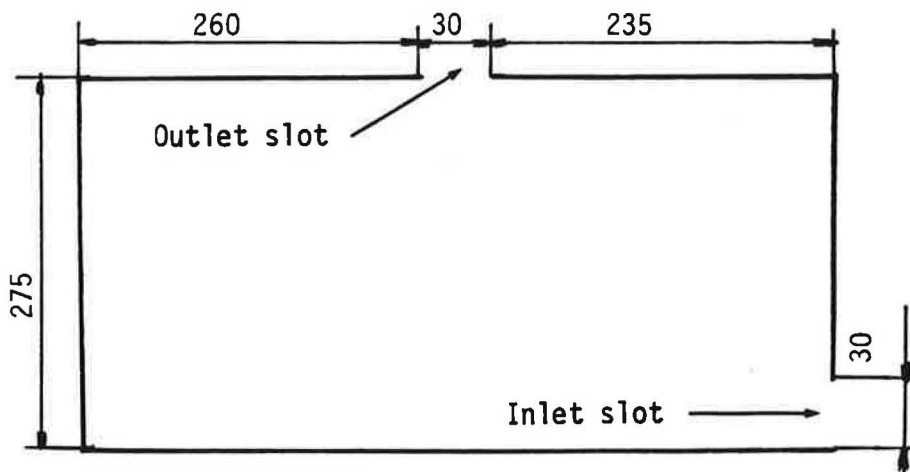


Fig 2 : Geometrical structure of the measuring plane P

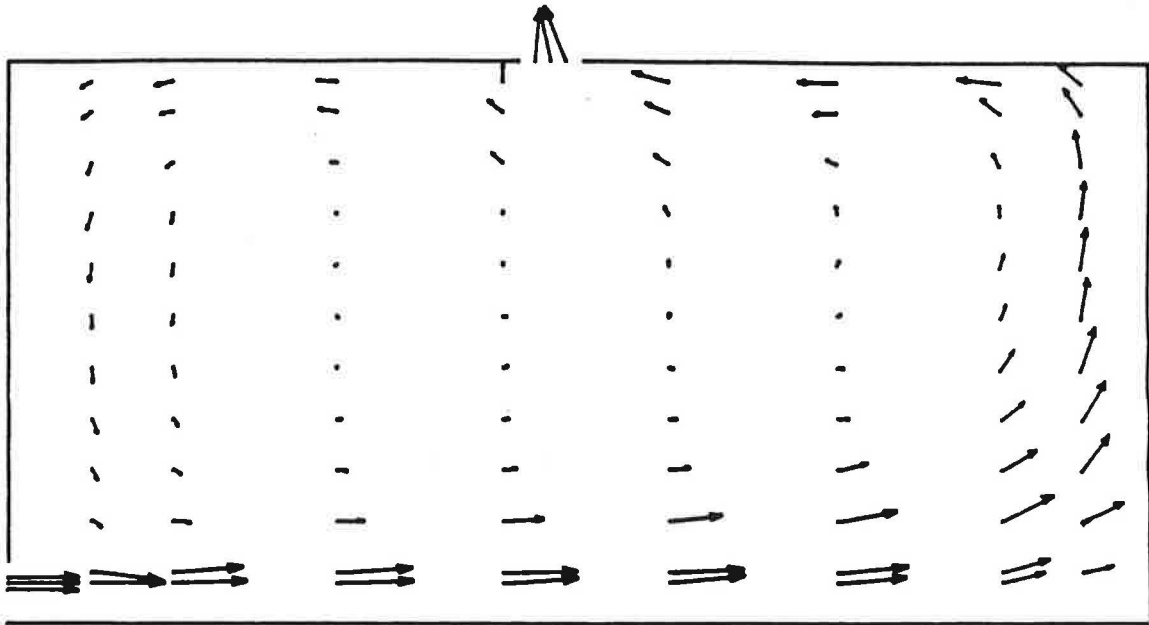


Fig 3 : The experimental mean velocity field

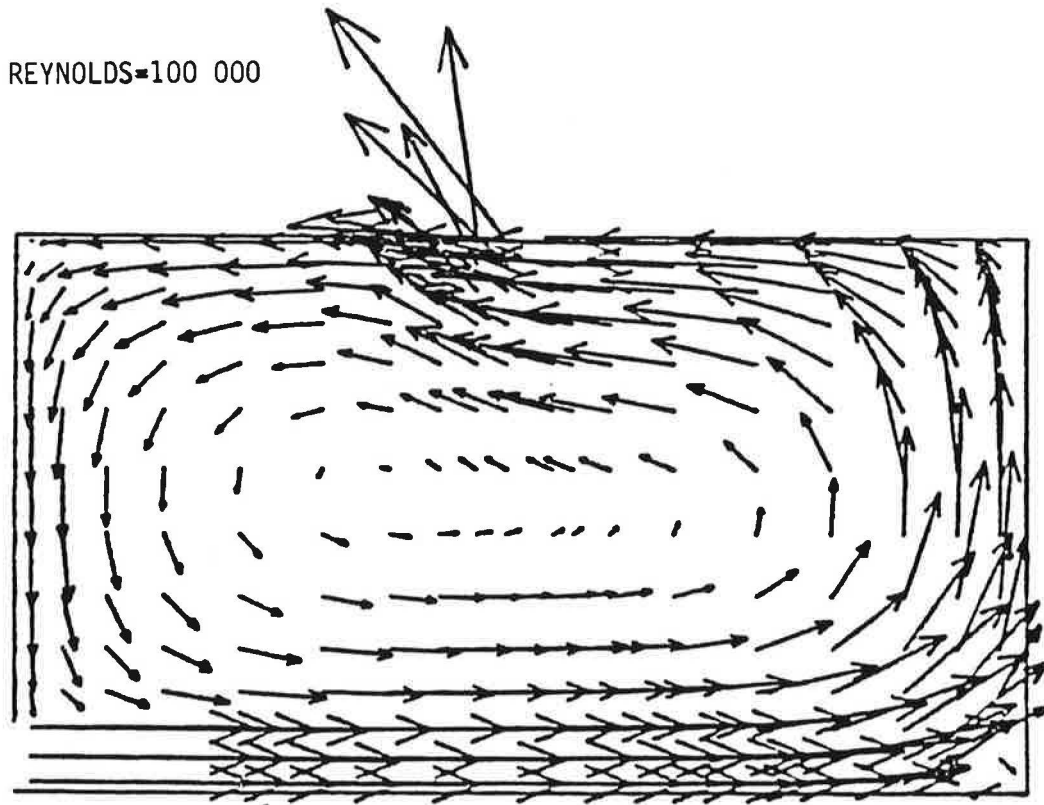


Fig 4 : Computed velocity field

X (mm)	Y (mm)	U_x (cm/s)	U_z (cm/s)	U_z/U_x (%) ^x
76	25	23,41	2,39	10
152	25	23,16	2,30	9
228	25	24,71	2,42	10
304	25	22,44	1,06	5
380	25	21,70	0,57	3
456	25	13,23	0,15	1
494	25	6,01	2,23	37

Table 5 : Accuracy of the two-dimensional mean flow hypothesis in the wall jet

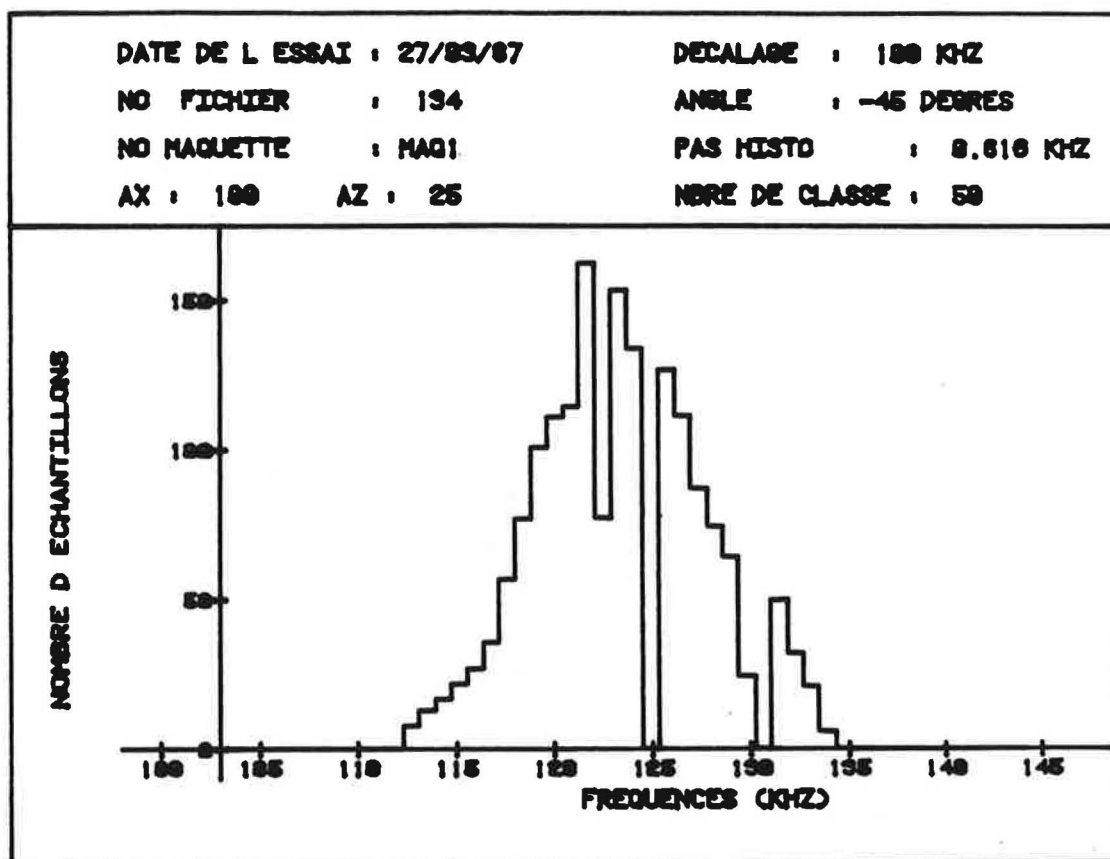


Fig 6 : Space distribution of the Doppler frequencies
 $[X = 100 \text{ mm}, Z = 25 \text{ mm}, \alpha = -45^\circ]$

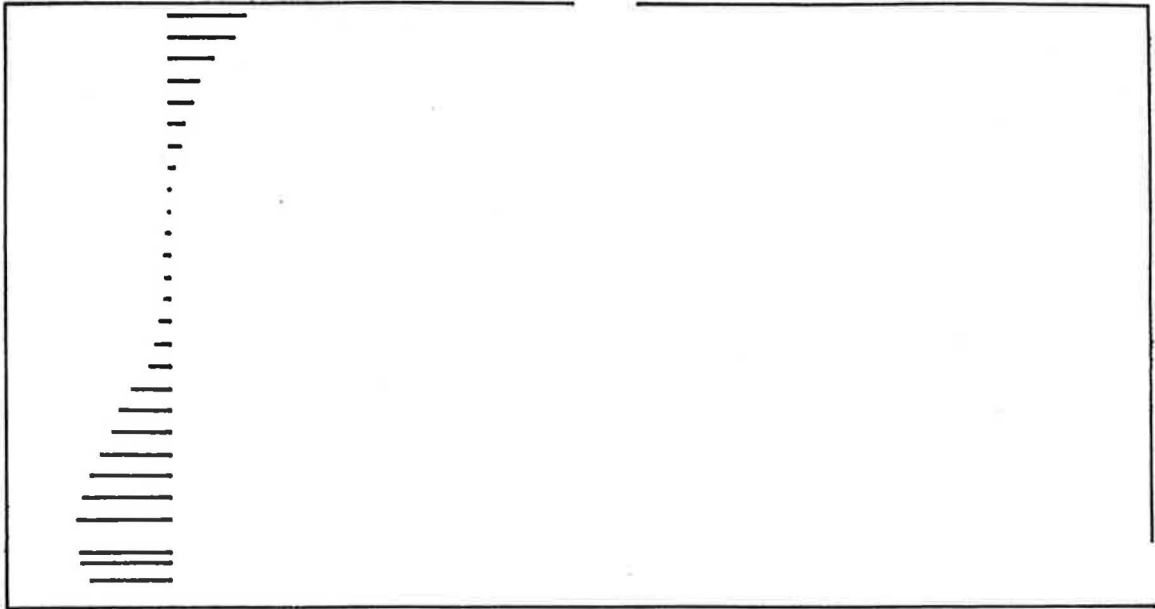


Fig 7 : Distribution of the U mean velocity component along the vertical line [X = 450 mm]

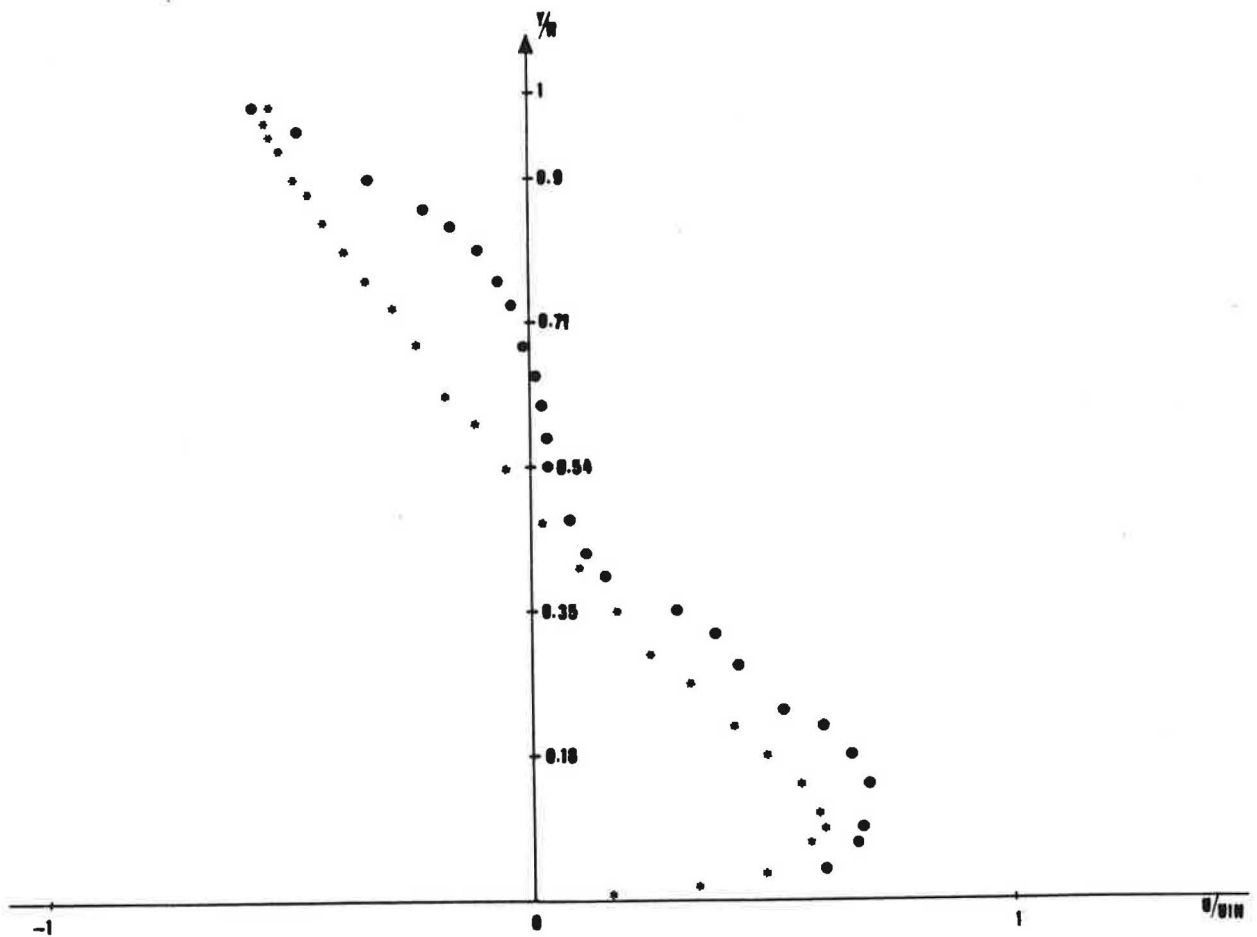


Fig 8 : Comparison between adimensional experimental (●) and numerical (*) vertical profiles at X = 450 mm